Available online at www.sciencedirect.com
ScienceDirect
ISA Transactions 46 (2007) 459–469
www.elsevier.com/locate/isatrans

MIMO variable structure controller design for a bioreactor benchmark process

M.Ö. Efe*

TOBB Economics and Technology University, Department of Electrical and Electronics Engineering, Sogutozu Cad. No 43, 06560, Sogutozu, Ankara, Turkey

Received 29 September 2006; accepted 19 March 2007
Available online 22 May 2007

Abstract

In this paper, variable structure control of a bioreactor is studied. The process has two state variables named cell mass and nutrient amount, and two control inputs to maintain the state variables at their desired levels. Although the state space representation of the system seems simple, the system displays several challenges that make it necessary to develop a good flowrate (control) management strategy. Due to the plant-model mismatch, variable structure control technique is applied and it is seen that the sliding subspace is reached in finite time and the behavior thereafter is insensitive to considerable degrees of variation in the parameters and disturbances. The design is based on the nominal model and a comparison with a feedback linearizing controller is presented. The objective of the paper is to illustrate the efficacy of MIMO sliding mode control on a benchmark problem. Overall, the results with the proposed controller demonstrate the following desirable characteristics: (i) very good tracking precision (ii) small percent overshoot values and (iii) good decoupling of the process states.

Keywords: Bioreactor benchmark problem; Nonlinear control; Process control

1. Introduction

Chemical processes often display a complicated behavior due to the strong interdependencies between the variables involved. Although in some cases the process is described by a few state variables, obtaining good disturbance rejection with high tracking precision requires implementing nonlinear control laws. The performance obtained with nonlinear control laws cannot be achieved in general by utilizing their counterparts designed through the use of linearized or simplified models of the process. This aspect of chemical processes makes them good test beds for benchmarking. A review of nonlinear control techniques on chemical processes is presented in [4], where the feasibility and efficacy of nonlinear control laws are discussed with an emphasis on relevant control challenges encountered in chemical process engineering.

Ungar [18] defines a Bioreactor Benchmark Problem that excellently fits in the context. The state of the process is described by two dimensionless variables named the cell mass denoted by $c_1(t)$ and the amount of nutrients denoted by $c_2(t)$ (see [18]). In [16,8], the single input version of the problem is addressed. The goal in that problem setting is to maintain only the cell mass at desired levels while keeping the nutrient amount bounded by altering the sole input of the reaction, which is the pure water feed stream. Ungar [18] defines a further complicated version of the single input setting by equipping the reaction tank with another incoming flow, which is the concentrated substrate feed stream. Thus the problem turns into a multivariable control problem where the values of cell mass and nutrient amount can be set independently. The sum of the inflow streams in the Multi Input Multi Output (MIMO) control problem is equal to the outflow value, hence the reaction volume is kept constant during the course of operation. The challenges associated with the control of this process are the nonlinearity enabling the emergence of a rich set of dynamical regimes, instabilities caused even by tiny variations in the process variables and the presence of a long control sampling interval in the feedback loop.

In the past, the single input version of this process was used several times for modeling and feedback control purposes. Efe et al. [8] consider this problem for developing a nonlinear

* Tel.: +90 312 2924064; fax: +90 312 2924180.
E-mail address: onderefe@etu.edu.tr.

0019-0578/$ - see front matter © 2007, ISA. Published by Elsevier Ltd. All rights reserved.
doi:10.1016/j.isatra.2007.03.005

control law forcing the process states to those of a first order linear one. Feedforward neural networks are used to build the nonlinear function in the control law and the plant is forced to follow a reference model. Puskorius and Feldkamp [16] study this problem in the context of demonstrating the efficacy of a neural network learning algorithm and consider the control problem about a setpoint in the stable region, another setpoint in the unstable region and a transition between these regions. The controller proposed in our study is able to keep the system states in the unstable region as will be discussed in the following. In [2], the bioreactor benchmark problem was used in the justification of state dependent modeling approach. Brengel and Seider [5] propose a multi step nonlinear controller based on predictive control theory and validate the performance of the closed loop control system on a variant of the model considered here. The authors of that work emphasize the preferability of operating at highest possible cell mass solutions, which are desired to be reasonably away from the region of periodic oscillations. Fossas et al. [9] discuss the design of a sliding mode controller for the single input version of the process considered here and follow the equivalent control approach whereas we consider reaching law approach (see [12] for details). In [3], it is emphasized that the controller design even for the single input bioreactor benchmark problem is a challenge due to the nonlinearity and a set of complicated regimes that arise due to it. Clearly, the works mentioned above motivate us to position the merit and effectiveness of Variable Structure Control (VSC) techniques in the control of continuously stirred tank reactors. In this paper, we consider the MIMO control problem and analyze the limitations of the design carried out with a thorough discussion.

Variable Structure Control (VSC), also known as Sliding Mode Control (SMC), is a well established approach ensuring some degrees of robustness against uncertainties in the feedback loop. The underlying idea is to create a sliding subspace, which is an attractor due to the philosophy of the design, [12,19]. SMC technique, which has many successful applications in motion control systems, is also applied for feedback control of chemical processes. See for example [10], where the process under investigation is modeled by a partial differential equation, [6], where the design is based on a first order model including dead time, and [7], where a second order sliding mode control is performed after feedback linearization. In [1], the technique is used in devising an uncertainty observer acting in a process control loop. One fact in all these studies needs emphasis: The sliding mode controller drives the system toward the sliding manifold and maintains the behavior on that loci, which is stable by the design and the error converges the origin of the phase space. Once the trajectories are confined to the sliding manifold, the control system displays some degrees of robustness against disturbances and parameter variations in system dynamics. This response is called invariance property of sliding mode control, [13,14,12]. The underlying idea in this paper is to implement a robust controller for the bioreactor benchmark problem. The reaching law approach in [12] is followed in the design.

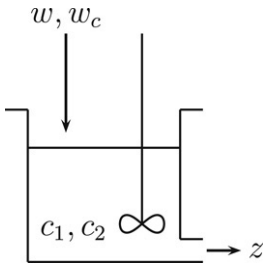

Fig. 1. Reaction tank with equal inflow and outflow rates.

This paper is organized as follows. Section 2 introduces the bioreactor benchmark problem and analyzes its behavior. Section 3 emphasizes the main result of this work with the design of the nonlinear feedback control laws. Section 4 is devoted to the operating conditions, simulation results and their interpretations. The concluding remarks are given at the end of the paper.

2. Bioreactor benchmark problem

The bioreactor considered in this study is a tank in which the biological cells are mixed with nutrients, water and substrate as shown in Fig. 1. The cells and nutrients are in a dynamical interaction modeled by (1) and (2), where $c_1(t)$ denotes the dimensionless cell mass while $c_2(t)$ stands for the dimensionless nutrient amount. The process is continuously fed by pure water and concentrated substrate. The variable characterizing the feed stream for pure water is denoted by $w(t)$ whereas the substrate concentration is tuned by altering $w_c(t)$. In order to maintain the reaction volume constant, the contents of the tank are removed at a rate denoted by $z(t)$, which is equal to the sum of the water and substrate feed streams. The goal of the multivariable control problem is to achieve the tracking of independent desired temporal profiles for the cell mass and for the nutrient amount. The state variables of the process and the nominal model seen below are assumed to be available for constructing the controller.

$$\dot{c}_1(t) = -c_1(t)\,(w(t) + w_c(t)) + c_1(t)\,(1 - c_2(t))\,\mathrm{e}^{\frac{c_2(t)}{\gamma_n}} \tag{1}$$

$$\dot{c}_2(t) = -c_2(t)\,(w(t) + w_c(t)) + c_1(t) \times (1 - c_2(t))\,\mathrm{e}^{\frac{c_2(t)}{\gamma_n}}\,\frac{1+\beta_n}{1+\beta_n - c_2(t)} + \mu_n w_c(t) \tag{2}$$

where the state variables are constrained by $\Omega := 0 \leq c_1(t), c_2(t) \leq 1$ and the feed streams $0 \leq w(t), w_c(t) \leq 2$. In the nominal model of the plant given above, the growth rate is characterized by the parameter $\beta_n = 0.02$ and the nutrient inhibition parameter is given by $\gamma_n = 0.48$. In (2), $\mu_n = 2$ is the substrate feed stream gain. A subscript n indicates the nominal value of the subscripted variable.

In Fig. 2, several trajectories are shown for a set of initial conditions denoted by a circle. Each subplot depicts the evolution of the system at a constant set of inflow streams indicated on the top. Depending on the value of the inflow streams, the attractors change their locations and new attractors emerge as well. As seen from the top right subplot of Fig. 2, one visible one is a limit cycle which becomes apparent when

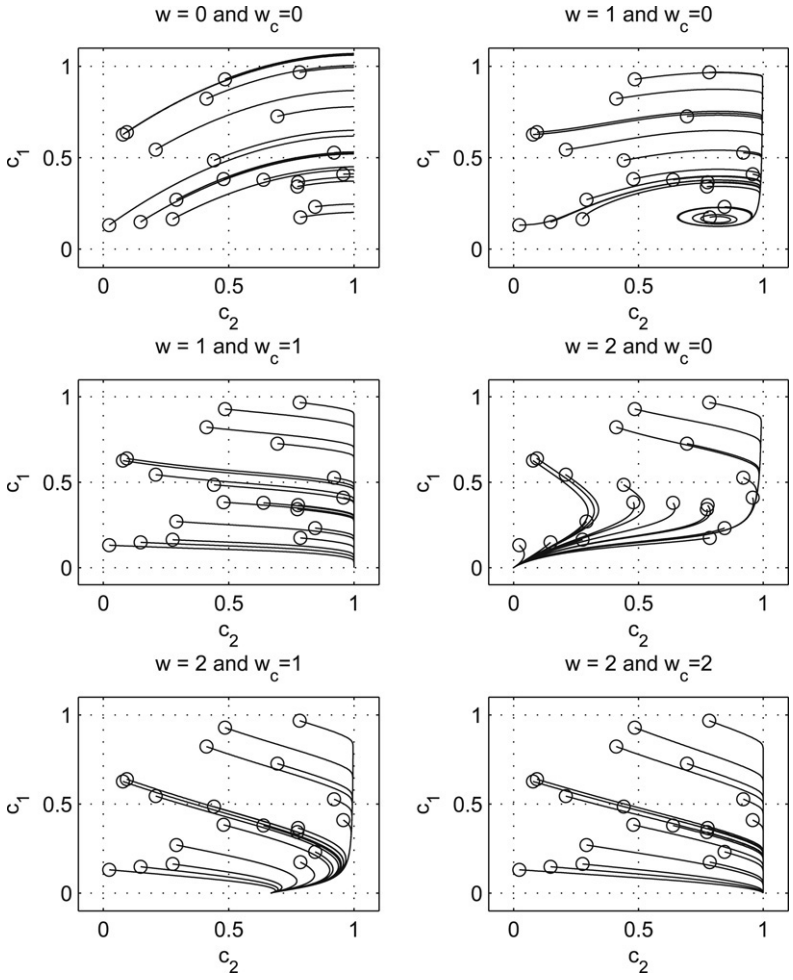

Fig. 2. The evolution of the process state for different initial conditions and at different feed streams. The trajectories are for 80 s time.

$w = 1$ and $w_c = 0$. When $w = 0.8290$ and $w_c = 0$, the system changes its qualitative behavior radically. Computing the equilibrium values corresponding to this pair of inflow streams, one obtains $c_1 = 0.1331$ and $c_2 = 0.8626$. The eigenvalues of the linearized system of equations at this point stipulate that the system undergoes Hopf bifurcation at this operating point and turns into an unstable one displaying spontaneous oscillations due to the limit cycle. In this regime, cell mass varies in between 0.1219 and 0.1466 while the nutrient amount fluctuates in between 0.8243 and 0.8996. At the points of crossing the imaginary axis, the eigenvalues of the linearized model are approximately equal to $0 \pm j1.7543$, from which we infer that the self sustained oscillations are quite fast.

A closer look at the subplots of Fig. 2 unfold the following facts: The state vector of the unforced process dynamics ($w = 0$, $w_c = 0$) terminates at a point on $c_2 = 1$ boundary of Ω. When $w = 1$ and $w_c = 0$, a limit cycle is created as seen in the top right subplot. This emphasizes that the system state lies strictly within Ω. Physically, the cases $w = w_c = 1$ and $w = w_c = 2$ converge the equilibrium, where $c_2 = 1$ and $c_1 = 0$, i.e. within the tank, there are too much nutrients but no cells to feed. In other words, the reaction is overfed. The case with $w = 2$ and $w_c = 0$ terminate at the origin of the state space, i.e. no cells and no nutrients are available in the reaction tank, i.e. the water feed stream is dominant and extinction of the cells is the inevitable result. The bottom left subplot of the figure demonstrates that the system states converge to an attractor, on which cell mass is zero but some amount of nutrients in between 0.5 and unity is available.

In Fig. 3, the aforementioned limit cycle and the convergence of some neighboring trajectories are illustrated for $w = 1$ and $w_c = 0$. In fact, limit cycles can occur for all values of admissible feed streams, i.e. $0 \leq w, w_c \leq 2$. According to Bendixson theorem (see [17,15]), since the quantity

$$\begin{aligned} H :=& \frac{\partial}{\partial c_1}\left(-c_1(w+w_c)+c_1(1-c_2)\mathrm{e}^{\frac{c_2}{\gamma_n}}\right) \\ &+ \frac{\partial}{\partial c_2}\left(-c_2(w+w_c)+c_1(1-c_2)\mathrm{e}^{\frac{c_2}{\gamma_n}}\right. \\ &\left.\times \frac{1+\beta_n}{1+\beta_n-c_2}+\mu_n w_c\right) \\ =& -2(w+w_c)+h(c_1,c_2) \end{aligned} \tag{3}$$

does not vanish and does not change sign in $\Lambda \subseteq \Omega$, no limit cycles can exist entirely in Λ. For a given constant pair of feed stream values, the curve of sign change for H is moved to the curve described by $h(c_1, c_2) = 2(w + w_c)$. Therefore one should run the quantity $2(w + w_c)$ from 0 to 8 and

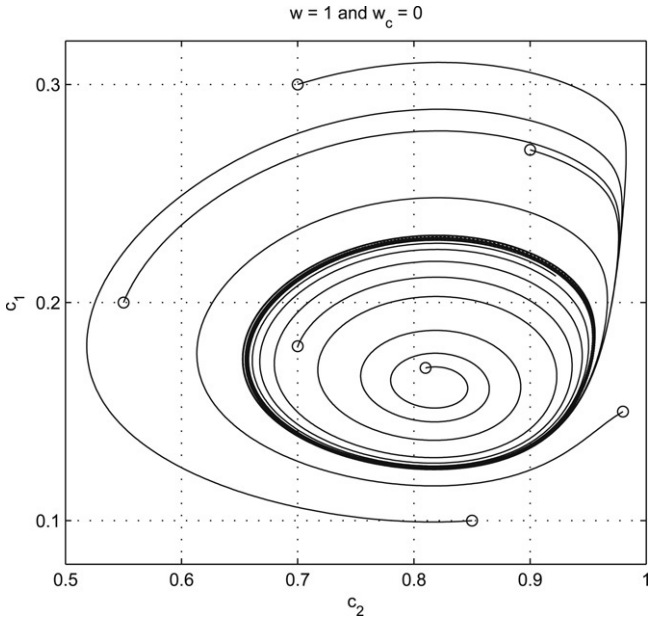

Fig. 3. Limit cycle arising when $w = 1$ and $w_c = 0$.

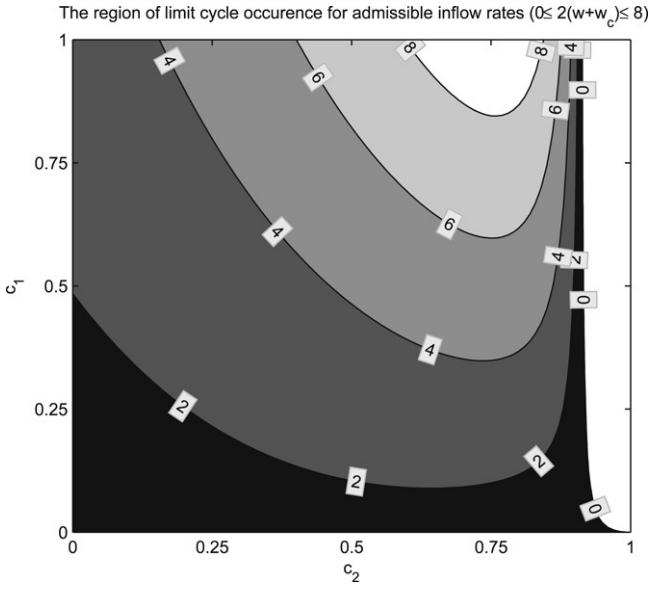

Fig. 4. Regions where limit cycles cannot occur are designated by white color.

determine where the sign change occurs. In Fig. 4, the regions where the limit cycles cannot lie entirely within are depicted as white regions, termed Λ above, and the value of $2(w + w_c)$ is contoured for $2(w + w_c)$ equal to 0, 2, 4, 6 and 8. According to this result, we figure out that it is possible to have other limit cycle trajectories in the system dynamics and $\Omega \setminus \Lambda$ is a significantly wide subspace of Ω. From the control engineering point of view, this practically tells us that during the controlled operation of the process, many attractors and/or repellers can be created or destroyed depending on the values of w and w_c, and the controller must be overcoming the dynamical influence of such difficulties while meeting the performance specifications and revealing disturbance rejection.

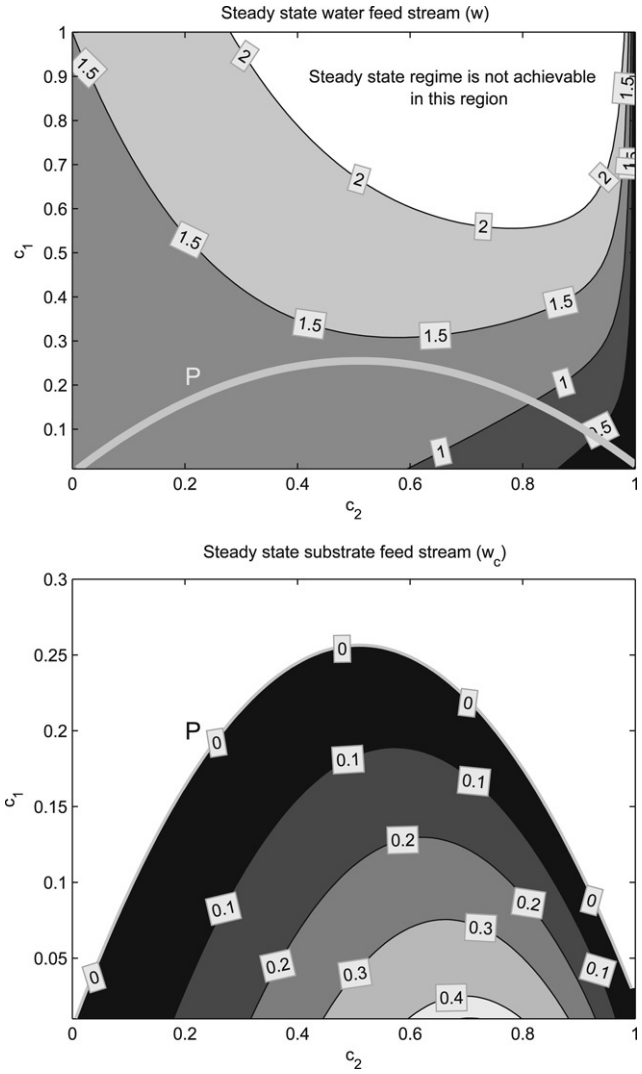

Fig. 5. Contour plots for steady state feed streams. Non-white regions indicate the existence of admissible feed stream values to maintain the system at an equilibrium. The region below the curve P is the intersection of the non-white and admissible regions in both subplots. The steady state values on or below the curve P are maintainable without violating the input constraints.

Now consider the process at the steady state, i.e. $\dot{c}_1 = 0$ and $\dot{c}_2 = 0$. This yields the steady state control actions given by

$$w_{ss} = \left(\frac{1}{c_1} + \frac{1}{\mu_n}\left(g - \frac{c_2}{c_1}\right)\right) f \tag{4}$$

$$w_{c\,ss} = -\frac{1}{\mu_n}\left(g - \frac{c_2}{c_1}\right) f \tag{5}$$

where

$$f := c_1(1 - c_2)\mathrm{e}^{\frac{c_2}{\gamma_n}} \tag{6}$$

$$g := \frac{1 + \beta_n}{1 + \beta_n - c_2}. \tag{7}$$

With these control signals, the system is at an equilibrium. The stability of the equilibrium states with the constraints on the feed streams let us generate the plots in Fig. 5, where the top subplot indicates the location of steady state water feed stream

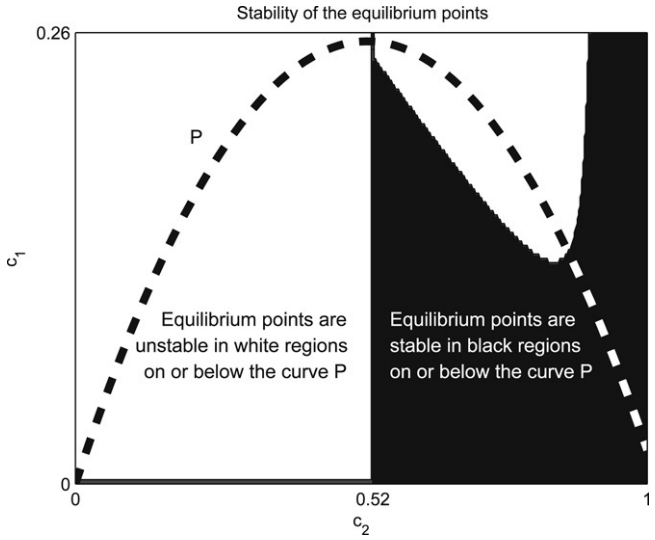

Fig. 6. The stability of the equilibrium states.

value as the state vector moves within Ω. Particular values are contoured and it is seen that there are no equilibrium states for some subregion of Ω as w is constrained by $0 \leq w \leq 2$.

Similarly in the bottom subplot of Fig. 5, we see that the admissible values of the equilibrium states are below a parabolic curve labeled by a symbol P, on which the steady state substrate feed stream value is zero and above this curve, negative w_c values are needed to maintain the system at the equilibrium point. The same parabolic curve is also indicated in the top subplot to clarify the regions in which the equilibrium states are maintainable by admissible feed stream values.

In Fig. 6, stability of the equilibrium values are shown. The stability conclusion is drawn by linearizing the plant at every particular operating point. Since these equilibrium values are achievable only on or below the curve P, we focus on that particular subspace of Ω. According to the figure, unstable equilibrium points indicated by white regions while the black region is the region where equilibrium points are stable. Particularly along the vertical line $c_2 = 0.52$, the eigenvalues of the linearized system are both equal to zero which make it necessary to consider higher order terms to draw a stability conclusion.

A last point that should be emphasized is the effect of sampling in the control loop. In [18], the equation system in (1) is discretized by the Euler method and a step size $\Delta = 0.01$ s is used. The sampling period for the control signal, called macro time steps [16] is equal to 50Δs, which is long enough for the bioreactor process to develop deviations and spontaneous oscillations from a desired setpoint or a trajectory. In this paper, we test the performance of the proposed controller by operating it at a prolonged rate, 60Δs.

Ungar [18] points out that although this system is not a completely realistic model of any bioreactor, as seen from the presented discussion, the system considered in this paper displays several challenges highlighted also by Anderson and Miller [3] with a similar motivation. Due to the presented properties of the system, the model constitutes a good candidate for scrutinizing the merits and effectiveness of conventional nonlinear control laws as emphasized by Ungar [18].

3. Main result: MIMO sliding mode control of the bioreactor

Theorem 3.1. *Let $r_1(t)$ and $r_2(t)$ be independently chosen differentiable desired profiles for the cell mass $c_1(t)$ and the nutrient amount $c_2(t)$, respectively. Let $e_1(t) := r_1(t) - c_1(t)$ be the error in the cell mass and $e_2(t) := r_2(t) - c_2(t)$ be the error in the nutrient amount. Let $s_1(t) := e_1(t)$ and $s_2(t) := e_2(t)$ be the switching variables and define the zero dimensional sliding subspace (sliding manifold) for i-th state variable by $s_i(t) = 0$, $i = 1, 2$. With $\zeta_i, \eta_i > 0$ and the nominal plant nonlinearities $f(\cdot,\cdot)$ and $g(\cdot)$, the two control laws describing the pure water feed rate and the substrate feed rate given by*

$$w(t) = -\frac{c_2 - \mu_n}{c_1 \mu_n}\left(f - \dot{r}_1 + \zeta_1 \operatorname{sgn}(s_1) + \eta_1 s_1\right) + \frac{1}{\mu_n}\left(f \cdot g - \dot{r}_2 + \zeta_2 \operatorname{sgn}(s_2) + \eta_2 s_2\right) \tag{8}$$

$$w_c(t) = \frac{c_2}{c_1 \mu_n}\left(f - \dot{r}_1 + \zeta_1 \operatorname{sgn}(s_1) + \eta_1 s_1\right) - \frac{1}{\mu_n}\left(f \cdot g - \dot{r}_2 + \zeta_2 \operatorname{sgn}(s_2) + \eta_2 s_2\right) \tag{9}$$

ensure hitting the sliding subspace in finite time and the errors in both state variables are maintained around the origin of the corresponding sliding subspace.

Remark 1. Note that for the phase space of each state variable we have $s_i(t) \in \Re^1$, therefore, the sliding subspace is a point in $\Re^0$. In other words, the origin of the phase space $\Re^1$ coincides with the sliding subspace by the definition of $s_i(t)$.

Proof. Consider the nominal representation seen in (1) and (2) and choose the Lyapunov function candidate

$$V = \frac{1}{2}s_1^2 + \frac{1}{2}s_2^2. \tag{10}$$

The time derivative of the Lyapunov function in (10) is given by

$$\begin{aligned}\dot{V} &= \dot{s}_1 s_1 + \dot{s}_2 s_2 \\ &= (\dot{r}_1 - \dot{c}_1)\, s_1 + (\dot{r}_2 - \dot{c}_2)\, s_2 \\ &= (\dot{r}_1 - (-c_1\,(w + w_c) + f))\, s_1 \\ &\quad + (\dot{r}_2 - (-c_2\,(w + w_c) + f \cdot g + \mu_n w_c))\, s_2\end{aligned} \tag{11}$$

where f and g are defined in (6) and (7), respectively. Substituting the proposed pair of inflow rates given by (8) and (9) into (11), one obtains

$$\begin{aligned}\dot{V} &= (-\zeta_1 \operatorname{sgn}(s_1) - \eta_1\, s_1)\, s_1 + (-\zeta_2 \operatorname{sgn}(s_2) - \eta_2\, s_2)\, s_2 \\ &= -\zeta_1 |s_1| - \zeta_2 |s_2| - \eta_1 s_1^2 - \eta_2 s_2^2 \\ &= < 0.\end{aligned} \tag{12}$$

In particular, we have $\dot{s}_i = -\zeta_i \operatorname{sgn}(s_i) - \eta_i\, s_i$ resulting in $\dot{s}_i s_i = -\zeta_i |s_i| - \eta_i s_i^2 < 0$ and all trajectories are attracted by the locus described by $s_i = 0$, $i = 1, 2$. Once the trajectories are

confined to the locus $s_i = 0$, then they converge to the origin. The proof of this is straightforward.

Note that when hitting occurs, $s_i(t_{h,i}) = 0$ and $\dot{s}_i(t_{h,i}) = 0$ are satisfied. Here, $t_{h,i}$ denotes the hitting time for the i-th state, i.e. the time elapses till a nonzero initial value $s_i(0)$ reaches the sliding subspace.

$$s_i(t_{h,i}) = s_i(0) - \int_0^{t_{h,i}} \zeta_i \,\mathrm{sgn}(s_i(\tau)) + \eta_i\, s_i(\tau)\,\mathrm{d}\tau. \tag{13}$$

The quantity $\mathrm{sgn}(s_i(t))$ is constant and does not change sign until the time of hitting. Therefore we have

$$s_i(t_{h,i}) = s_i(0) - \mathrm{sgn}(s_i(0)) \int_0^{t_{h,i}} \zeta_i + \eta_i\,|s_i(\tau)|\,\mathrm{d}\tau = 0. \tag{14}$$

Or alternatively

$$\mathrm{sgn}(s_i(0)) \left(|s_i(0)| - \int_0^{t_{h,i}} \zeta_i + \eta_i\,|s_i(\tau)|\,\mathrm{d}\tau \right) = 0. \tag{15}$$

Paraphrasing and rearranging (15) yields

$$|s_i(0)| = \int_0^{t_{h,i}} \zeta_i + \eta_i\,|s_i(\tau)|\,\mathrm{d}\tau \geq \int_0^{t_{h,i}} \zeta_i\,\mathrm{d}\tau = \zeta_i\, t_{h,i}. \tag{16}$$

The hitting time $t_{h,i}$ satisfies $t_{h,i} \leq \frac{|s_i(0)|}{\zeta_i}$, which puts a finite upper bound on the time interval for reaching the sliding subspace, i.e. $e_i(t) = 0$ is reached in finite time. Once the system is in the sliding mode, the motion is confined to the sliding subspace thereafter. This result guarantees that the desired state profiles are followed. □

For a detailed discussion on the relevance of SMC technique and the types of switching functions, handling of parasitic dynamics and steady state behaviors, one should refer to [19,17,20,11].

In the derivations presented so far, we have assumed that when the sliding mode starts, $s_i = 0$ and $\dot{s}_i = 0$ are satisfied. Yet in the application domain, it is difficult to encounter these idealized conditions due to the plant-model mismatch and inevitable disturbances. Practically, due to the infinite gain when $s_i = 0$, unnecessarily fast switching control signals are produced and very small variations in s_i can provoke this phenomenon, which is highly undesired. This is called *chattering* and is a prime drawback of sliding mode control systems. A significant number of research studies addressed obtaining chattering free sliding control, and one practical solution is to introduce a boundary layer using a function that is smooth around $s_i = 0$ instead of the sign function (see [17, 6] and the references therein). Among other alternatives, in this study, we adopt the following widespread approximation with $\delta > 0$ for smoothing the switching element.

$$\mathrm{sgn}(s_i) \approx \frac{s_i}{|s_i| + \delta}. \tag{17}$$

The function in (17) resembles the original sign function as δ gets closer to zero. Conversely, the discontinuity of the sign function is changed into a very smooth transition as δ gets larger. In the next section, we discuss the details regarding the justification of the proposed controller.

4. Operating conditions, results and discussion

The true process considered in justifying the analytical claims is given in (18) and (19), where the variables x_1 and x_2 correspond to the true values of the state variables c_1 and c_2, respectively.

$$\begin{aligned}\dot{x}_1(t) &= -x_1(t)\,(w(t) + w_c(t)) + x_1(t) \\ &\quad \times (1 - x_2(t))\,\mathrm{e}^{\frac{x_2(t)}{\gamma(t)}} + d_1(t)\end{aligned} \tag{18}$$

$$\begin{aligned}\dot{x}_2(t) &= -x_2(t)\,(w(t) + w_c(t)) + x_1(t)\,(1 - x_2(t))\,\mathrm{e}^{\frac{x_2(t)}{\gamma(t)}} \\ &\quad \times \frac{1 + \beta(t)}{1 + \beta(t) - x_2(t)} + \mu(t) w_c(t) + d_2(t)\end{aligned} \tag{19}$$

$$c_1(t) = x_1(t) + \varepsilon_1(t) \tag{20}$$

$$c_2(t) = x_2(t) + \varepsilon_2(t). \tag{21}$$

According to the procedure introduced, the control laws in (8) and (9) are realized under the following operating conditions and plant-model mismatch issues.

- The observations for the state variables $c_1(t)$ and $c_2(t)$ are noisy. The Gaussian noise sequences corrupting the state variables lie within the interval $[-0.0156, 0.0156]$ with a probability very close to unity. The noise in the observations is a difficulty influencing the closed loop control performance adversely. We utilize the following partial observer for suppressing the effect of noise on $c_1(t)$;

$$\begin{aligned}\hat{c}_1(t) &= -\hat{c}_1(t)(w(t) + w_c(t)) + \hat{c}_1(t)(1 - c_2(t))\mathrm{e}^{\frac{c_2(t)}{\gamma_n}} \\ &\quad + K(c_1(t) - \hat{c}_1(t))\end{aligned} \tag{22}$$

  where $K > \sup_{c_2 \in [0,1]}(1 - c_2(t))\mathrm{e}^{\frac{c_2(t)}{\gamma_n}}$ makes it sure that the time derivative of the Lyapunov function $W = \frac{1}{2}(c_1 - \hat{c}_1)^2$ is negative definite if $c_1(t) \neq \hat{c}_1(t)$. It is straightforward to show that this observer removes the spurious content from the measured value of $c_1(t)$. During the tests, the inflow rates entering the observer dynamics are corrupted by zero mean noise sequences, which lie in between ± 0.02.

  We study the noisy measurements in $c_2(t)$ too. Due to the tedious stability proof, we leave the alleviation of the difficulties caused by this fact to the controller instead of utilizing an observer for $c_2(t)$ dynamics.

  According to the above discussion, we exploit $\hat{c}_1(t)$ and $c_2(t)$ as the state variables in constructing the control signals in (8) and (9).
- In [18], it is emphasized that small variations from the nominal values γ_n and β_n lead to significant deviations from the target cell mass for the single input problem setting. For example, given perfect state measurements, 2% change in γ_n and 20% change in β_n may cause 50% deviation in the cell mass, $c_1(t)$, (see [5,18]). In this paper, we consider the nominal values of these parameters for the design of the controller and in the justification of the proposed scheme, we study these parameters with some variation in time. The necessity for investigating the behavior under parameter variations is tightly relevant to the need of exploring the controller performance under extreme conditions. The top

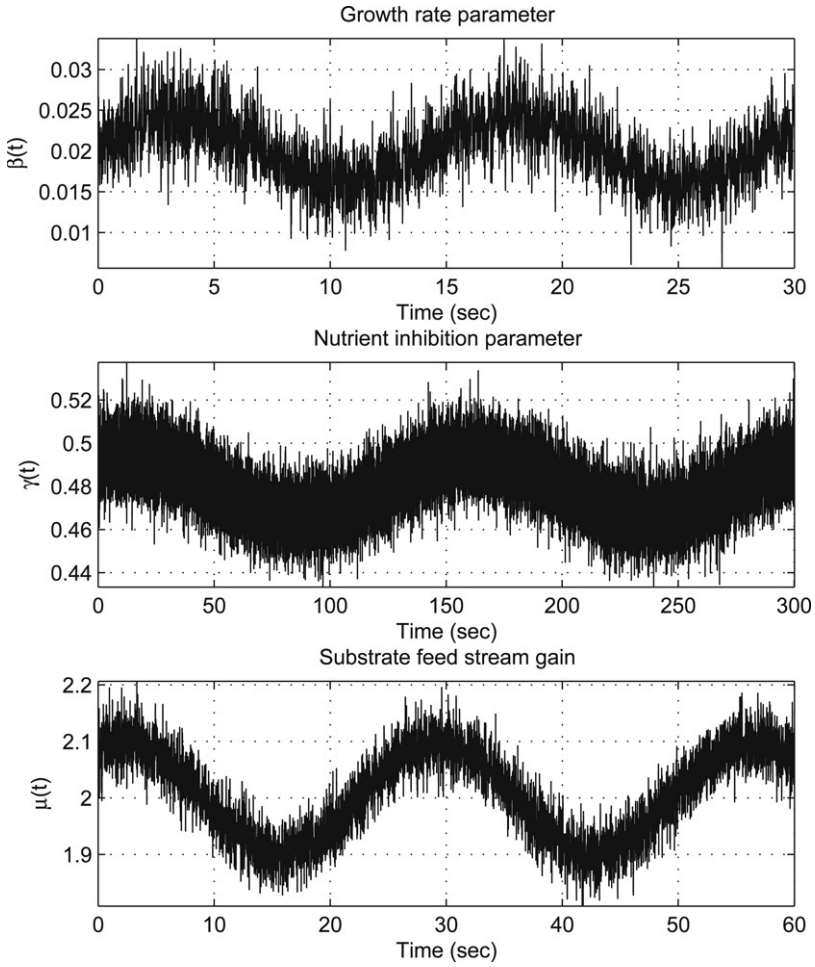

Fig. 7. The evolution of nutrient inhibition parameter ($\gamma(t)$) and growth rate parameter ($\beta(t)$) and substrate gain ($\mu(t)$).

subplot of Fig. 7 depicts the change of growth rate parameter, $\beta(t)$ for a period of 30 s. The evolution of this parameter displays a variation in $[0.1276\,,\ 3.7543] \times 10^{-2}$ indicating a maximum of 93.62% deviation from the nominal value given by $\beta_n = 0.02$. Likewise, in the middle subplot of Fig. 7, $\gamma(t)$ is illustrated for the first 300 s of the simulation. The value of this variable changes within the interval $[0.4225\,,\ 0.5375]$, which means maximum 12% change from the nominal value of the nutrient inhibition parameter (γ_n). Lastly, the value of substrate feed stream gain changes as shown in the bottom subplot of Fig. 7, where the deviation from the nominal value $\mu_n = 2$ is at most 11.87%.

- Two other sources of disturbance are indicated by $d_1(t)$ in (18) and $d_2(t)$ in (19), which are absent in the nominal model. In the justification phase, random signals satisfying $-0.15 \leq d_1(t), d_2(t) \leq 0.15$ are utilized.

  Clearly the variations in $\beta(t)$, $\gamma(t)$ and $\mu(t)$, the presence of measurement noise and the presence of other disturbance terms require certain degrees of robustness to meet the stability and performance requirements.
- Another difficulty is the large initial errors in the state variables. If $e_1(0)$ and $e_2(0)$ are large, then the designed controller must force them toward zero with a sequence of admissible feed streams, $w(t)$, $w_c(t)$, while maintaining the stability during the transient phase. This paper also addresses the issue of handling the large initial errors.
- The choice of the reference signal is another important issue in closed loop control. As shown in the top left subplot of Fig. 8, the desired cell mass (dashed curve) claims the management of three different regimes, namely the simulation is started with a trapezoidal profile that lasts 800 s, continued with a sinusoidal profile for another 800 s and finally we choose a discontinuous desired profile to see how the controller stabilize the system at different cell mass levels during $1600 \leq t \leq 3200$ s. The whole course of the desired nutrient amount is to follow a sinusoidal reference profile with offset equal to 0.4 and amplitude and frequency are 0.15 Hz and 0.005 Hz respectively.

  Aside from the numerical details given above, the reference signal $r_1(t)$ is chosen according to the facts presented in Fig. 5, where the equilibrium states are maintainable with admissible feed streams only on or below the curve P. This obviously puts an upper bound to the desired values of cell mass as $r_1(t) < \frac{1+\beta_n}{4} = 0.255$. According to the same figure, the mean value of the nutrient amount can be increased yet in that case the state c_2 might get trapped to the attractor at $c_2 = 1$. This is better seen in Fig. 2, where most trajectories have a tendency either to pass closely or toward the region described by $c_2 = 1$.

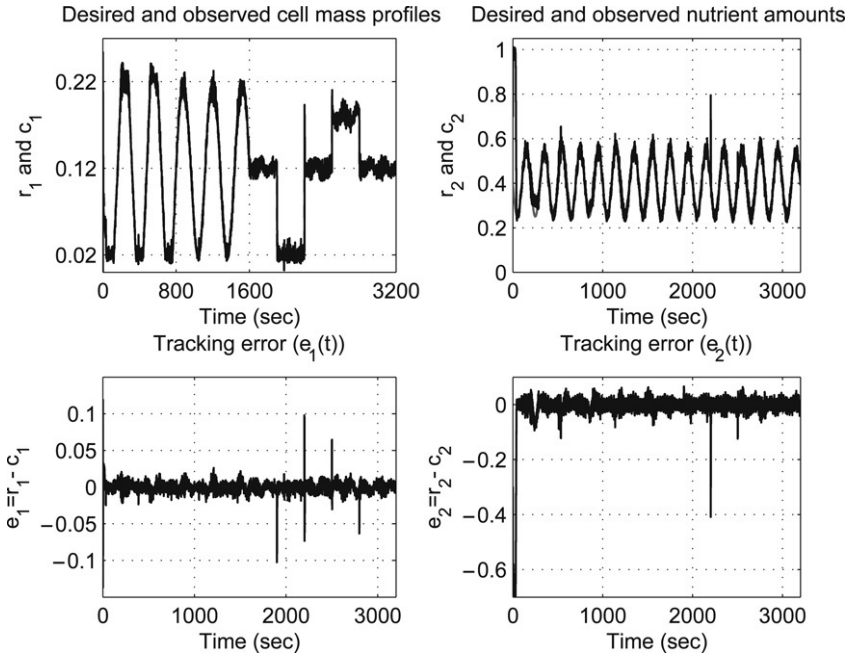

Fig. 8. The evolution of the cell mass and the nutrient amount for the given desired profiles are illustrated with the tracking error.

- Finally, the effect of actuation interval for the controller will be emphasized. Ungar [18] defines $T = 50\Delta = 0.5$ s. as the control interval. In other words, the inflow streams maintain their values during $nT \leq t < (n+1)T$, where n is a discrete time index. Consequently, the computation of the control signals applied during this interval is based on the observations at $t = nT$. The practical drawback of such an actuation scheme is the following: As discussed in the second section and shown in Fig. 2, the system may get trapped to a limit cycle or an attractor during this time and this makes it necessary to implement a perfect flow rate management strategy. This paper adopts $T = 60\Delta = 0.6$ s. to further increase the practical applicability of the controller while making the control problem more demanding.

The other parameters of the SMC are $\zeta_1 = 0.06$, $\eta_1 = 0.01$, $\zeta_2 = 0.1$, $\eta_2 = 0.1$ and $\delta = 0.05$, which have been set after a few trials. As shown in the top subplots of Fig. 8, the state variables (solid curves) closely follow the desired profiles (dashed curves). The bottom subplots depict the discrepancy between the desired values and achieved values of the state variables, i.e. $e_1(t)$ and $e_2(t)$. The results seen emphasize that admissibly small tracking errors are maintained. When the initial transients are taken into consideration, we observe $t_{h,1} = 4.832$ s and $t_{h,2} = 42.4$ s, however the values set by Theorem 3.1 are $t_{h,1} \leq \frac{|s_1(0)|}{\zeta_1} \approx 1.33$ s and $t_{h,2} \leq \frac{|s_2(0)|}{\zeta_2} \approx 3.034$ s. We attribute these results to the presence of uncertainties and unmodeled dynamics effective during the justification phase. The use of (17) introduces a thin boundary layer whose thickness is determined by δ. If $s_i(t)$ is within the boundary layer, then it approaches the origin smoothly. This modification of the original pair of control laws is another reason of the delays in hitting. If the tests are carried out for the nominal system, it is seen that hitting the sliding subspace occurs much earlier than the computed time values and they satisfy the upper bound given in Theorem 3.1. Nevertheless, the hitting in our experiments occur slightly later and the motions thereafter take place in the vicinity of the origin of each sliding subspace as they attract all trajectories within the corresponding phase space.

A substantially important measure for practical applicability is the cost of physical realizability of the signals produced by the controller. The time evolution of the feed stream values yielding the results shown in Fig. 8 are illustrated in Fig. 9 and three essential merits of the presented MIMO sliding mode controller are highlighted below. First, although the signals seem to have fast fluctuations, 0.6 s of (control interval) macro time steps and the long course of the simulation indicate that the shown signals are admissibly smooth. Second, fluctuations observed at the instants when step changes occur at the command signals are convergent. Note that in Theorem 3.1, it is assumed that the command trajectories are differentiable. Choosing this sort of a command profile violates this assumption yet it enables us to monitor the momentary response against such sharp changes and the interaction of nutrient amount and cell mass dynamics. In the right subplots of Fig. 8, we see instant but stable peaks in the behavior of c_2 and e_2 due to the step changes in the desired cell mass profile. Third, the substrate feed stream (w_c) is saturated for very short periods at the level $w_c = 0$, and almost no saturations take place in the course of water feed stream (w) including the reaching phase. These are the prominent features associated with the controller.

According to the obtained results, the controller possesses highly desirable characteristics such as very good disturbance rejection capability and guaranteed tracking precision under the presence of uncertainties. From a practical point of view, smoothness of the control signal makes it possible to implement the control law with hardware having no or little extraordinary properties.

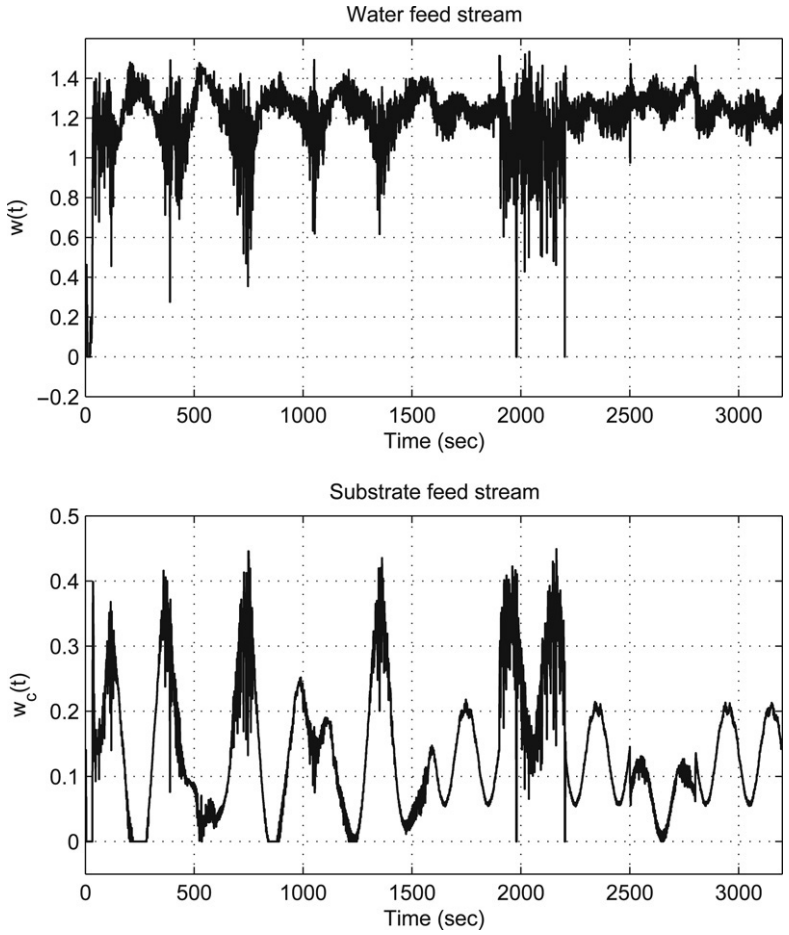

Fig. 9. The inflow rates generated by the proposed SMC.

One might wonder what happens if other values for ζ_is are used. According to the tests we have carried out, larger values of ζ_is provoke oscillations in the state variables. Larger values of η_is deteriorate the tracking performance significantly too. In fact, the choice of ζ_is is tightly dependent upon the quantity $\sup_{\hat{c}_1,c_2\in\Omega}|\Sigma_1|$ and $\sup_{\hat{c}_1,c_2\in\Omega}|\Sigma_2|$, where Σ_1 and Σ_2 denote the collective form of uncertainties when the control laws in (8) and (9) are substituted into the dynamics in (18)–(21). This would yield

$$\dot{s}_1 = -\zeta_1\,\mathrm{sgn}(s_1) - \eta_1 s_1 + \Sigma_1(c_1,\hat{c}_1,c_2,\varepsilon_1,\varepsilon_2,d_1,d_2,\gamma,\beta,\mu,\Delta) \quad (23)$$

$$\dot{s}_2 = -\zeta_2\,\mathrm{sgn}(s_2) - \eta_2 s_2 + \Sigma_2(c_1,\hat{c}_1,c_2,\varepsilon_1,\varepsilon_2,d_1,d_2,\gamma,\beta,\mu,\Delta). \quad (24)$$

It has been shown that the i-th sliding subspace is an attractor, i.e. $s_i\dot{s}_i < 0$ is satisfied if $|\Sigma_i| < \zeta_i$ holds true for $i = 1, 2$. In our case, the chosen values of ζ_i assure this condition without provoking any undesired oscillation in the state variables.

Finally, tests carried out with smaller values of the macro time steps have shown that the controller performs much better as the control interval is decreased yet this would require high sampling rates and fast computing facilities entailing costly hardware in practice.

For a comparison, since the functions f and g with the nominal parameter values are computable, we consider a Feedback Linearizing Controller (FLC).

Theorem 4.1. *Let $r_1(t)$ and $r_2(t)$ be independently chosen differentiable desired profiles for the cell mass $c_1(t)$ and the nutrient amount $c_2(t)$, respectively. Let $e_1(t) := r_1(t) - c_1(t)$ be the error in the cell mass and $e_2(t) := r_2(t) - c_2(t)$ be the error in the nutrient amount. With $\lambda_1, \lambda_2 > 0$, the two control laws describing the pure water feed rate and the substrate feed rate given by*

$$w(t) = \frac{f - \lambda_1 e_1(t)}{c_1(t)}\left(1 - \frac{c_2(t)}{\mu_n}\right) + \frac{f\cdot g - \lambda_2 e_2(t)}{\mu_n} \quad (25)$$

$$w_c(t) = \frac{c_2(t)}{c_1(t)\mu_n}(f - \lambda_1 e_1(t)) - \frac{f\cdot g - \lambda_2 e_2(t)}{\mu_n} \quad (26)$$

force the following globally exponentially stable closed loop dynamics

$$\dot{c}_1(t) = -\lambda_1(c_1(t) - r_1(t)) \quad (27)$$

$$\dot{c}_2(t) = -\lambda_2(c_2(t) - r_2(t)). \quad (28)$$

Proof. By direct substitution. □

Remark 2. In the above, $\lambda_1 > 0$ and $\lambda_2 > 0$ are the parameters that adjust the speed of response in each state variable. Though

Table 1
A comparison of the peak values and overshoot percentages at some particular instants of time

Time instant (t)(s)	r_b	r_a	$c_1(t_p)$ and M_p in SMC		$c_1(t_p)$ and M_p in FLC	
$t = 1900$	0.12	0.02	−0.1020	102%	−0.1020	102.0%
$t = 2200$	0.02	0.12	0.1932	73.2%	0.2200	100.0%
$t = 2500$	0.12	0.18	0.2103	50.5%	0.2565	127.5%
$t = 2800$	0.18	0.12	0.0633	79.1%	0.0636	79.5%

Table 2
A comparison of decoupling performances at some particular instants of time

Time instant (t)(s)	$e_2(t_p)$ in SMC	$e_2(t_p)$ in FLC
$t = 2200$	−0.4085	−0.6042
$t = 2500$	−0.1242	−0.2924

not specified in this problem setting, in practice, λ_1 and λ_2 are chosen according to the physical constraints such as time constants of the process and the actuation periphery.

FLC is tested under the identical operating conditions used with SMC. Although the tracking of the reference profiles yield similar results at a first glance, as seen from Table 1, SMC performs better in terms of overshoots caused by step changes in $r_1(t)$. We define the percent overshoot value for the problem in hand as follows

$$M_p = \frac{c(t_p) - r_a}{r_a - r_b} \times 100\% \tag{29}$$

where $c(t_p)$ is the quantity of interest at the peak time denoted by t_p, which is slightly later than the instant of step change. The value of the reference signal before the step is denoted by r_b and that after the step is r_a. According to these definitions, the computed values are summarized in Table 1.

A comparison in terms of the peak values and overshoot performances indicate that SMC performs better than FLC particularly at step-up instants. When the two sets of control laws are substituted into the system dynamics, one sees that both approaches have the goal of decoupling the cell mass dynamics and the nutrient amount dynamics from each other. However, the instant fluctuations observed in the nutrient amount coinciding with the step-up change times in the cell mass indicate that the two components of the reaction are not perfectly decoupled. Indeed, they cannot be perfectly decoupled with the chosen forms of the control laws due to 60Δ s of control sampling interval. In order to quantify the decoupling performance, we measure the maximal deviation from the desired value of the nutrient amount, i.e. the error $e_2(t_p)$ and tabulate the results given in Table 2. The observations with SMC emphasize that the behavior in the nutrient amount is less sensitive to instant changes in the cell mass response than that observed with FLC. This conclusion is due to the fact that the values with SMC are smaller in magnitude than the values with FLC.

Another comparison measure would be the variance of the error signals. For this purpose, we present the results in two tables, namely the ones concerning the whole course of the simulation in Table 3, and the one considering only after the reaching occurs in Table 4. Clearly the variances

Table 3
A comparison of the error variances for the whole course of the simulation

Variance	In SMC	In FLC
${\sigma_1}^2$	6.2736×10^{-5}	5.4715×10^{-5}
${\sigma_2}^2$	500×10^{-5}	94.356×10^{-5}

Table 4
A comparison of the error variances after hitting occurs

Variance	In SMC	In FLC
σ_1^2 ($t \geq 5$ s)	4.9725×10^{-5}	4.7582×10^{-5}
σ_2^2 ($t \geq 50$ s)	38.3400×10^{-5}	56.3890×10^{-5}

defined as ${\sigma_1}^2 = \text{var}\{e_1(t)\}$ and ${\sigma_2}^2 = \text{var}\{e_2(t)\}$ indicate that FLC performs better than SMC in producing smaller error variances including the initial transient, yet the results considering the periods after the hitting occurs do not show a dramatic difference.

The tabulated values of the observations with the result visualized in Fig. 8 indicate that the tracking performance, robustness, disturbance rejection capability and decoupling performance are worthwhile merits of the MIMO sliding mode controller.

5. Concluding remarks

This paper considers the MIMO sliding mode control of a chemical process exhibiting several difficulties for achieving and maintaining a satisfactory closed loop performance. The challenges associated with the plant are discussed and the derivation of a MIMO SMC is presented. The controlled variables are the cell mass and the nutrient amount within the tank and these variables are shown to follow desired profiles precisely. This is analyzed thoroughly and the theoretical claims are justified through simulations. It is observed that the feedback loop with the designed MIMO SMC displays insensitivity to the variations in the plant parameters, the noise in the measured quantities and disturbances. The results obtained with the sliding mode controller are compared with a feedback linearizing controller and it is seen that the SMC approach presented in this study performs better in terms of (i) decoupling the dynamics describing the behavior of the two state variables and (ii) smaller percent overshoot values compared to the FLC approach.

This paper differentiates from the existing body of literature in terms of (i) demonstrating how such a distinguishable degree of robustness can be observed with a design based on nominal plant dynamics, (ii) providing graphical results with physical interpretation of the conditions that are likely to occur

in practice, and finally (iii) postulating a fairly simple and low cost multivariable control law based on a reaching law approach of sliding mode control framework for a problem that is considered a challenging control problem in the literature.

Acknowledgments

This work was supported by TOBB Economics and Technology University, BAP Program, under contract no. ETÜ-BAP-2006/04.

The author gratefully acknowledges the facilities of the TOBB ETÜ library.

References

[1] Aquilar-Lopéz R, Alvarez-Ramiréz J. Sliding-mode control scheme for a class of continuous chemical reactors. IEE Proc Control Theory Appl 2002;149(4):263–8.
[2] Akesson BM, Toivonen HT. State-dependent parameter modelling and identification of stochastic non-linear sampled-data systems. J Process Control 2006;16:877–86.
[3] Anderson CW, Miller III WT. Challenging control problems. In: Miller III WT, Sutton RS, Werbos PJ, editors. Neural networks for control. MIT Press; 1990. p. 475–510.
[4] Bequette BW. Nonlinear control of chemical processes: A review. Ind Eng Chem Res 1991;30:1391–413.
[5] Brengel DD, Seider WD. Multistep nonlinear predictive controller. Ind Eng Chem Res 1989;28:1812–22.
[6] Camacho O, Rojas R. A general sliding mode controller for nonlinear chemical processes. Trans ASME: J Dyn Sys, Meas Control 2000;122: 650–5.
[7] Colantonio MC, Desages AC, Romagnoli JA, Palazoglu A. Nonlinear control of a CSTR: Disturbance rejection using sliding mode control. Ind Eng Chem Res 1995;34:2383–92.
[8] Efe MÖ, Abadoglu E, Kaynak O. A novel analysis and design of a neural network assisted nonlinear controller for a bioreactor. Int J Robust and Nonlinear Control 1999;9(11):799–815.
[9] Fossas E, Ros RM, Fabregat J. Sliding mode control in a bioreactor model. J Math Chem 2001;30(2):203–18.
[10] Hanczyc EM, Palazoglu A. Sliding mode control of nonlinear distributed parameter chemical processes. Ind Eng Chem Res 1995;34:557–66.
[11] Huang YJ, Wang YJ. Steady-state analysis for a class of sliding mode controlled systems using describing function method. Nonlinear Dynam 2002;30:223–41.
[12] Hung JY, Gao W, Hung JC. Variable structure control: A survey. IEEE Trans Ind Electron 1993;40(1):2–22.
[13] Kaynak O, Harashima F, Hashimoto H. Variable structure systems theory, as applied to sub-time optimal position control with an invariant trajectory. Trans Inst Electr Eng Japan E 1984;104:4752.
[14] Kaynak O, Harashima F. Disturbance rejection by means of a sliding mode. IEEE Trans Indust Electron 1985;IE-32:85–7.
[15] Khalil H. Nonlinear systems. New Jersey: Prentice Hall; 2001.
[16] Puskorius GV, Feldkamp LA. Neurocontrol of nonlinear dynamical systems with kalman filter trained recurrent networks. IEEE Trans Neural Netw 1994;5(2):279–97.
[17] Slotine J-JE, Li W. Applied nonlinear control. New Jersey: Prentice Hall; 1991.
[18] Ungar LH. A bioreactor benchmark for adaptive-network based process control. In: Miller III WT, Sutton RS, Werbos PJ, editors. Neural networks for control. MIT Press; 1990. p. 387–402.
[19] Utkin VI. Sliding modes in control optimization. New York: Springer Verlag; 1992.
[20] Young KD, Utkin VI, Özgüner Ü. A control engineer's guide to sliding mode control. IEEE Trans Control Sys Technol 1999;7(3):328–42.